Vps13-Mcp1 interact at vacuole–mitochondria interfaces and bypass ER–mitochondria contact sites

Arun T. John Peter,[1] Beatrice Herrmann,[1] Diana Antunes,[2] Doron Rapaport,[2] Kai Stefan Dimmer,[2] and Benoît Kornmann[1]

[1]ETH Zürich, Institute of Biochemistry, Zürich, Switzerland
[2]Interfaculty Institute of Biochemistry, University of Tübingen, Tübingen, Germany

Membrane contact sites between endoplasmic reticulum (ER) and mitochondria, mediated by the ER–mitochondria encounter structure (ERMES) complex, are critical for mitochondrial homeostasis and cell growth. Defects in ERMES can, however, be bypassed by point mutations in the endosomal protein Vps13 or by overexpression of the mitochondrial protein Mcp1. How this bypass operates remains unclear. Here we show that the mitochondrial outer membrane protein Mcp1 functions in the same pathway as Vps13 by recruiting it to mitochondria and promoting its association to vacuole–mitochondria contacts. Our findings support a model in which Mcp1 and Vps13 work as functional effectors of vacuole–mitochondria contact sites, while tethering is mediated by other factors, including Vps39. Tethered and functionally active vacuole–mitochondria interfaces then compensate for the loss of ERMES-mediated ER–mitochondria contact sites.

Introduction

In eukaryotic cells, exchange of membrane lipids between organelles is critical for sustaining their biogenesis and function. How lipids are exchanged with organelles that are not part of the vesicular transport network, such as mitochondria, remains unclear. Recent research stresses the importance of membrane contact sites (MCSs), zones of close proximity (10–30 nm) between two organellar membranes, as a means of nonvesicular lipid exchange between organelles (Helle et al., 2013; Phillips and Voeltz, 2016). In yeast and other fungi, an MCS between the ER and mitochondria is constituted by the ER–mitochondria encounter structure (ERMES). This protein complex consists of an ER transmembrane protein, Mmm1; a mitochondrial outer membrane protein, Mdm10; and two peripheral membrane proteins, Mdm12 and Mdm34 (Kornmann et al., 2009; Ellenrieder et al., 2016). ERMES tethers the ER to mitochondria, and three of its four core components bind lipid molecules through a tubular lipid–binding domain. Tubular lipid domains can extract lipid molecules from a membrane, shelter them from the cytosol, and deliver them to another membrane, thus acting as membrane lipid transporters (Kopec et al., 2010; Schauder et al., 2014; AhYoung et al., 2015; Jeong et al., 2016).

Despite this seemingly crucial role in mitochondrial membrane biogenesis, ERMES deficiency is not lethal and does not completely block lipid delivery to mitochondria (Kornmann et al., 2009). This is likely due to the existence of redundant pathways. One such pathway involves the formation of an MCS between the mitochondria and the vacuole. This MCS can be readily evidenced by the overexpression of the vacuolar fusion factor Vps39, which leads to the formation of extensive vacuole and mitochondria patches (vCLAMPs; Elbaz-Alon et al., 2014; Hönscher et al., 2014). The tethering of these two organelles is mediated by Vps39, the vacuolar Rab GTPase Ypt7, and a hypothetical mitochondrial factor. Simultaneous inactivation of ERMES and Vps39 is lethal and strongly reduces mitochondrial lipid import (Elbaz-Alon et al., 2014).

Therefore, a likely role for the ER–mitochondria MCSs is to deliver lipids to mitochondria from the ER, a function that is shared by vacuole–mitochondria MCSs. However, the compensation by redundant pathways is only partial because mutations that impair ERMES lead to a host of mitochondrial phenotypes. This suggests that redundant pathways are able to provide lipids to the mitochondria but are probably insufficient to completely compensate for the loss of ERMES.

Interestingly, the phenotypes associated with ERMES deficiency can be reverted by the overexpression of two mitochondrial proteins, Mcp1 and Mcp2, or by single amino acid substitutions in Vps13 (Tan et al., 2013; Lang et al., 2015; Park et al., 2016). Both Mcp1 and Mcp2 are integral membrane proteins that reside on the outer and inner mitochondrial membrane, respectively, and their molecular functions remain unclear. Vps13 is a conserved ∼360-kD protein that localizes to endosomes, to vacuole–mitochondria and mitochondria–endosome contact sites, and, upon glucose starvation, to the nuclear–vacuole junctions (Lang et al., 2015; Park et al., 2016). *MCP1*, *MCP2*, and

Correspondence to Benoît Kornmann: benoit.kornmann@bc.biol.ethz.ch

Abbreviations used: ERMES, ER–mitochondria encounter structure; MCS, membrane contact site; PH, Pleckstrin homology; PI3K, phosphatidylinositol-3 kinase; PK, proteinase K; SD, synthetic dextrose; ts, temperature-sensitive; vCLAMP, vacuole and mitochondria patch.

The Rockefeller University Press
J. Cell Biol. Vol. 216 No. 10 3219–3229
https://doi.org/10.1083/jcb.201610055

VPS13 are all synthetically lethal with the loss of ERMES, indicating that they function in ERMES-redundant pathways.

Together, this suggests that ERMES-redundant pathways can be boosted to render ERMES entirely dispensable. Yet whether Mcp1, Mcp2, and Vps13 function at mitochondria–vacuole contacts is unclear. The fact that *VPS13* suppressor allele can exert its suppressive functions only in the presence of Vps39 and Mcp1, but independent of Mcp2 (Lang et al., 2015), suggests that Vps13, Mcp1, and Vps39 might constitute one coherent unit to mediate the tethering and function of vacuole–mitochondria MCSs and ensure cell survival in the absence of the ERMES complex. Here we investigate the relationship among Mcp1, Vps13, and Vps39. We show that Mcp1 recruits Vps13 to mitochondria and vCLAMPs and that this recruitment underlies the functionality of vacuole–mitochondria contacts in the ERMES bypass pathway. Our data support a model in which Vps39 and its binding partners establish tethering between mitochondria and vacuole, whereas Mcp1 and Vps13 participate in the functional output of mitochondria–vacuole contact sites to restore cellular growth and homeostasis.

Results

To address in an unbiased manner how Vps13 is involved in bypassing ERMES function, we inspected two published genetic interaction datasets (Costanzo et al., 2010; Hoppins et al., 2011). Synthetic genetic screens involve the creation of double-deletion strains, monitoring their growth, and computing genetic interaction scores. A highly powerful way to analyze genetic interaction data is to compute correlations between profiles of genetic interactions (Collins et al., 2010) in which strong positive correlations are typically indicative of a common function. According to Costanzo et al. (2010), the gene that best correlated with *VPS13* was *VPS38*, and the second best was *VPS30* (Fig. 1 A). In the dataset of Hoppins et al. (2011), which did not contain *VPS38*, the best-correlated gene was *VPS30* (Fig. 1 A). Both Vps30 and Vps38 are part of the phosphatidylinositol-3 kinase (PI3K) complex II, together with Vps34 (Kihara et al., 2001), which was absent from both datasets. The PI3K complex II is important for vacuolar protein sorting and is targeted to endosomes and vacuole by Vps38 (Obara et al., 2006). The link between Vps38/Vps30 and Vps13 in protein sorting along the endocytic pathway is further supported by a recent study showing that Vps13 is necessary for transport between trans-Golgi and late endosomes (De et al., 2017). Moreover, a hidden Markov model–based homology prediction uncovered a putative Pleckstrin homology (PH)–like domain at the extreme C terminus of Vps13 (Fig. 1 B and Alignments S1–S3; Söding et al., 2005; Fidler et al., 2016). The strong correlation with PI3K complex II subunits along with the presence of a PH-like domain at the C terminus of Vps13 suggests a nexus between Vps13 and the endocytic pathway via phosphatidylinositol-3-phosphate. Indeed, Vps13 localizes to Vps38-positive early endosomes (Huh et al., 2003; Fig. 2 A).

We hypothesized that Vps38 may recruit Vps13 to the endosomes either by itself or via phosphatidylinositol-3-phosphate. To directly test this idea, we deleted *vps38* in a strain expressing a functional GFP-tagged Vps13 (Vps13^GFP; Lang et al., 2015). To our surprise, Vps13 remained on FM4-64-positive, defective endosomes found in *vps38Δ* cells (Fig. 1 C; Luo and Chang, 1997). This observation suggested that Vps13 requires

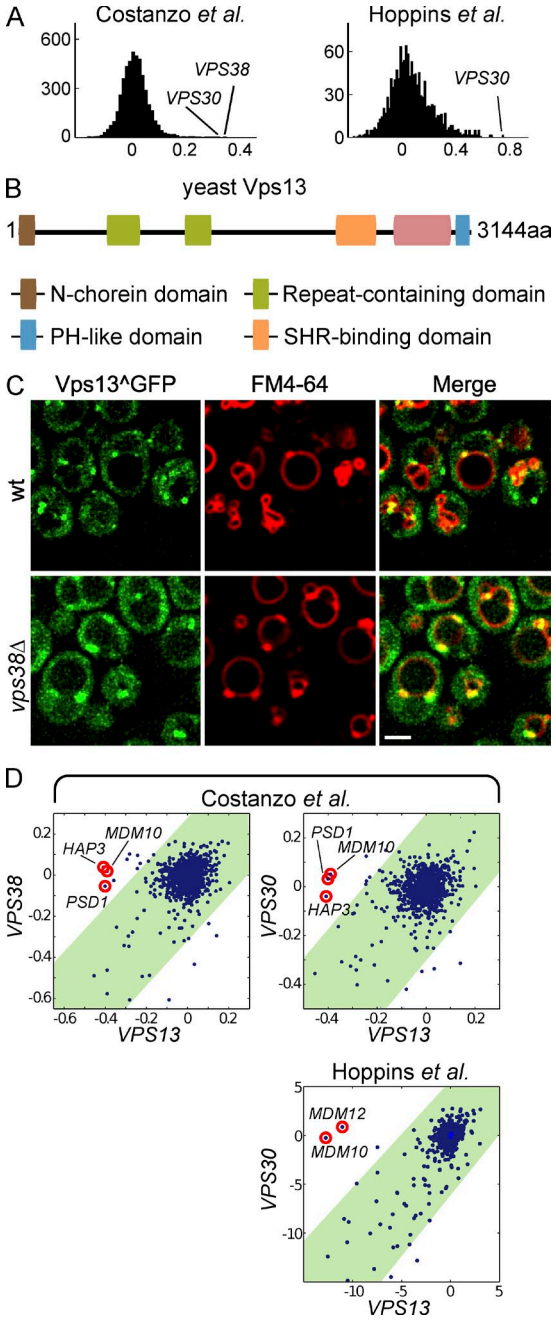

Figure 1. **The function of Vps13 on endosomes is unlinked to its function in ERMES suppression.** (A) Correlation analysis of the genetic interactions of *VPS13*. Correlation coefficients were calculated for the genetic interaction profile of *VPS13* and all genes present in the Costanzo et al. (2010) dataset (left) and Hoppins et al. (2011) dataset (right). (B) Domain architecture of yeast Vps13. Repeat-containing domains are mapped according to Velayos-Baeza et al. (2004). Predictions were made using a hidden Markov model–based homology search (HHPred; Söding et al., 2005). A PH-like domain was detected at the C terminus (3,037–3,133 aa) when searched against the Protein Data Bank. (C) Vps13 remains on endosomes in *vps38Δ* cells. Localization of GFP-tagged endogenous Vps13 in WT and *vps38Δ* cells. Vacuoles and endosomes are stained with FM4-64. Bar, 2 µm. (D) Genetic interaction profile of *VPS13* (x axis) plotted against *VPS38 and VPS30* (y axis; left and middle) using data from Costanzo et al. (2010). (Right) The profile of *VPS13* versus *VPS30* using data from Hoppins et al. (2011). The correlation in the genetic interaction profiles of *VPS13* with that of both *VPS30* and *VPS38* is highlighted by the green area. Genes encoding ERMES members as well as *PSD1* and *HAP3* are circled in red when present.

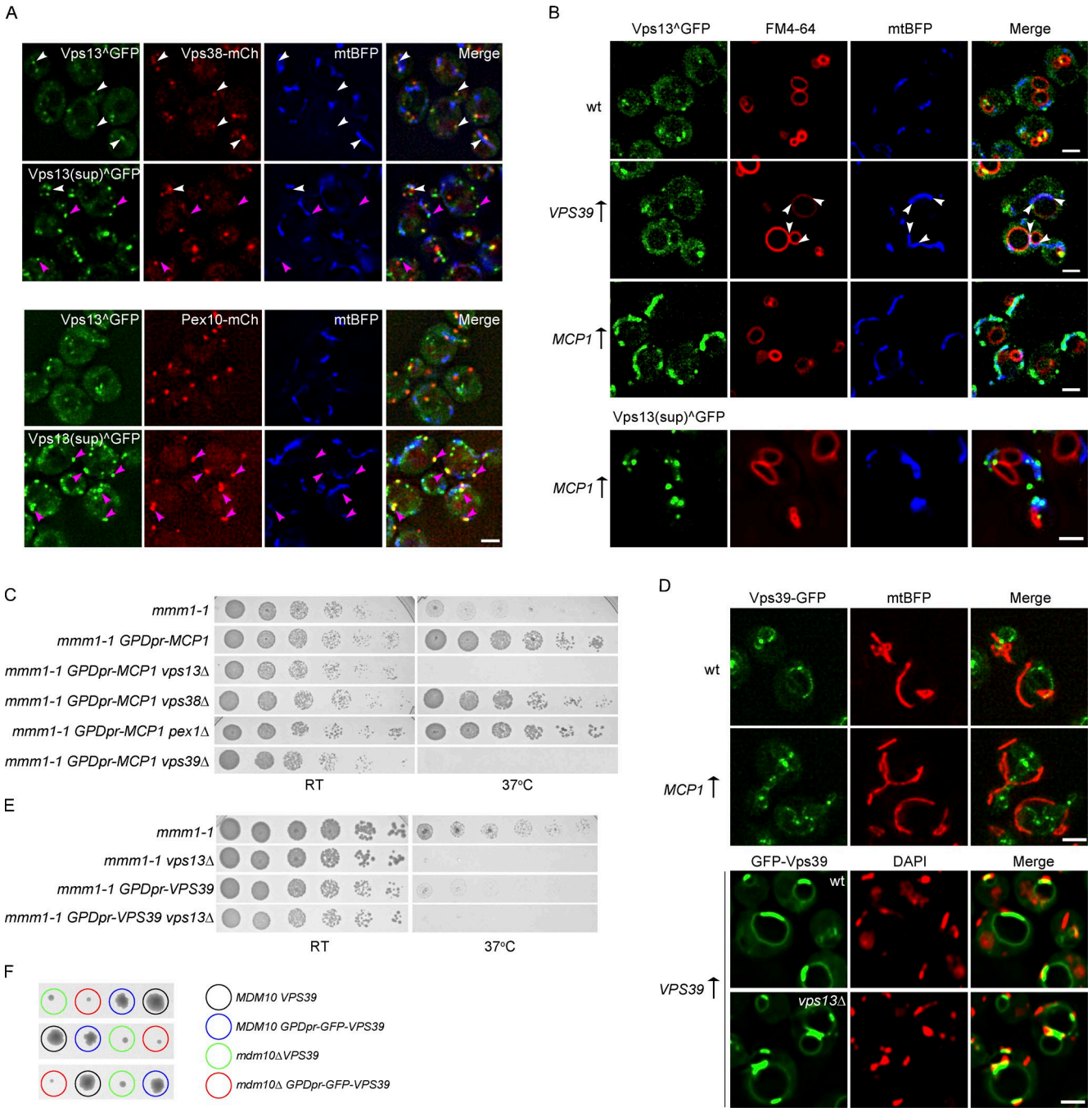

Figure 2. **Relationship between Vps13 and suppressors of ERMES defects.** (A, top) Localization of internally GFP-tagged Vps13 (WT or suppressor; Vps13 bearing the internal GFP tag that retains its functionality is depicted as Vps13^GFP) with mCherry-tagged Vps38 expressed from endogenous promoters. Mitochondria are marked by a plasmid-encoded, matrix-targeted BFP (mtBFP). White and pink arrowheads mark Vps13 foci that do or do not colocalize with Vps38, respectively. (Bottom) Localization of GFP-tagged Vps13 (WT or suppressor) with mCherry-tagged Pex10 expressed from endogenous promoters. Pink arrowheads point at Vps13 foci that colocalize with peroxisomes marked by Pex10-mCherry. Bar, 2 µm. (B) Localization of endogenous Vps13 under normal conditions or upon overexpression of Vps39 or Mcp1 (*VPS39*↑ and *MCP1*↑, respectively). Vacuoles are stained with FM4-64. Bars, 2 µm. Arrowheads indicate vacuole–mitochondria patches (vCLAMPs). The Vps13 suppressor version is expressed from a low-copy plasmid, under the control of its native promoter. (C) Mcp1-mediated growth rescue requires both Vps13 and Vps39. The ts strain *mmm1-1* with the indicated genotypes was spotted as serial dilutions on yeast extract peptone dextrose plates and grown either at RT or 37°C. (D, top) Maximum intensity projection of five Z-sections showing the localization of endogenous GFP-tagged Vps39 (green) in WT and Mcp1-overexpressing cells. Mitochondria are marked by mtBFP (shown in red). (Bottom) WT or *vps13Δ* cells expressing GFP-tagged Vps39, from the strong GPD promoter, were stained with DAPI to visualize mitochondrial DNA (shown in red). Bars, 2 µm. (E) Vps39 overexpression does not rescue temperature-induced dysfunction of ERMES subunit Mmm1. Strains with the indicated genotype were spotted as in C. (F) Tetrad dissection of sporulated *MDM10/mdm10Δ VPS39/GPDpr-GFP-VPS39* diploids. Genotype of individual spores is indicated with color-coded circles.

neither Vps38 nor phosphatidylinositol-3-phosphate, made by PI3K complex II, to localize to endosomes. Furthermore, the analyses of genetic interaction datasets also showed that despite the strong similarity in the genetic interaction profiles of *VPS13*, *VPS38*, and *VPS30*, several genes had synthetic genetic interactions with *VPS13* only (Fig. 1 D). These genes encode members of the ERMES complex (*MDM10* and *MDM12*) and other factors associated with mitochondrial function, including *PSD1*, encoding phosphatidylserine decarboxylase, which makes phosphatidylethanolamine from phosphatidylserine at the inner mitochondrial membrane, and HAP3, a transcriptional regulator of respiratory gene expression (Mattoon et al., 1990). Collectively, we conclude that Vps13 functions in the endocytic pathway in a way that correlates with PI3K complex II but that this function is probably separable from its role in substituting the functions of the ERMES complex.

Because Vps13 function in the ERMES bypass pathway appeared disconnected to its role at the endosome, we reasoned that the ability of Vps13 to suppress ERMES function might be linked to an alternative subcellular localization. We colocalized Vps13 with different organellar markers in various ERMES-suppressing conditions. We assessed Vps13 localization when it bore a suppressing mutation (L1627S), when vacuole–mitochondria MCSs were exacerbated into vCLAMPs by Vps39 overexpression, and upon Mcp1 overexpression. As expected, in normal conditions, a majority (60 ± 1.7%, mean ± SEM) of the Vps13 foci colocalized with the endosomal marker Vps38 (Fig. 2 A, top). In contrast, a much smaller fraction (17.5 ± 0.8%) of Vps13 bearing the suppressor mutation localized to Vps38-positive foci. To address the localization of remaining foci, we performed colocalization with different organellar markers (not depicted) and found that these foci mostly corresponded to peroxisomes (Fig. 2 A, bottom). Indeed, in contrast to 6.8 ± 1.6% of WT Vps13 foci, 41.1 ± 1.23% of the Vps13 suppressor foci localized to Pex10-positive peroxisomes. We also observed that Pex10-positive peroxisomes only seldom (0.43 ± 0.28%) colocalized with Vps38-positive endosomes (Fig. S1). Upon Vps39 overexpression, there was no change in the localization of Vps13 (Fig. 2 B, *VPS39*↑), even though large vCLAMPs, indicative of vCLAMP formation, could be seen (arrowheads). Intriguingly, when Mcp1 was overexpressed, Vps13 relocalized to mitochondria. The relocalization was also observed for the suppressor allele, but in a more dotted fashion (Fig. 2 B, *MCP1*↑). Thus, whereas a suppressor mutation induces the relocalization of Vps13 to peroxisomes, Mcp1 overexpression induces the relocalization of both the Vps13 WT and suppressor mutant to mitochondria. Of note, vCLAMP induction has largely no effect on Vps13 localization.

As the ability of Mcp1 to suppress ERMES defects was in line with the dramatic localization phenotype of Vps13, we tested whether Mcp1 overexpression required *VPS13* to bypass ERMES function. To this end, we used the *mmm1-1* temperature-sensitive (ts) strain, which manifests the typical slow-growth phenotype of ERMES mutants at the restrictive temperature only. Overexpression of Mcp1 in this strain rescued the growth phenotype at 37°C, in accordance with published data (Tan et al., 2013). However, deletion of *vps13* completely abolished the ability of *MCP1* overexpression to rescue the loss of *MMM1* function (Fig. 2 C), suggesting that Vps13 recruitment to mitochondria is a critical event in the ERMES bypass pathway.

We also found that Vps38 was necessary neither for the Vps13- nor for the Mcp1-mediated rescue (Fig. 2 C and Fig. S2), confirming our earlier conclusion that Vps38 is not linked to the function of Vps13 in rescuing the loss of ERMES. (Fig. 1 D).

Our colocalization analysis also suggested that peroxisomes could be involved in the bypass pathway (Fig. 2 A). To test this genetically, we deleted pex1 in the *mmm1-1* ts strain overexpressing Mcp1. Cells lacking *PEX1*, a critical factor for peroxisomal biogenesis, lack functional peroxisomes and harbor only peroxisomal "ghosts" that do not have any matrix proteins (Knoops et al., 2015). Interestingly, Mcp1 overexpression rescued loss of *MMM1* function even in the absence of *pex1* (Fig. 2 C), indicating that functional peroxisomes are not necessary to bypass ERMES functions. Therefore, it is possible that the localization of the suppressor mutant to peroxisomes is an epiphenomenon unrelated to ERMES suppression.

Finally, we found that Vps39 was necessary for Mcp1 to rescue the *mmm1-1* growth defect (Fig. 2 C). This is consistent with the fact that Vps39 is also necessary for suppressor alleles of Vps13 to exert their suppressive function (Lang et al., 2015). However, Mcp1 overexpression, like the expression of Vps13 suppressor alleles (Lang et al., 2015), did not lead to visible Vps39-mediated vCLAMP formation (Fig. 2 D, top), and vCLAMP formation upon Vps39 overexpression was not dependent on the presence of Vps13 (Fig. 2 D, bottom). We then wondered if Vps39 overexpression-mediated vCLAMP formation was sufficient to rescue the loss of ERMES function. Because of the rapidity of suppressor accumulation in haploid strains bearing ERMES mutations, we used either a *mmm1-1* ts mutant or tetrad-dissected heterozygous diploid strains. Surprisingly, we found that vCLAMP formation mediated by Vps39 overexpression rescued neither the growth defect of a ts *mmm1-1* strain (Fig. 2 E) nor, contrary to published literature (Hönscher et al., 2014), of an *mdm10Δ* strain (Fig. 2 F). Actually, WT, *mdm10Δ*, and *mmm1-1* cells, overexpressing *VPS39* from the strong GPD promoter, grew slower than cells expressing *VPS39* from its endogenous promoter. Collectively, these results indicate that vCLAMPs induced by Vps39 overexpression are not sufficient by themselves to compensate for the loss of ERMES.

Because overexpression of Mcp1 clearly shifted most of the Vps13 signal to mitochondria, we wondered if Mcp1 might be a limiting binding partner for Vps13 on mitochondria. To address this, we coimmunoprecipitated HA-tagged Mcp1 together with either the WT or suppressor (L1627S) GFP-tagged Vps13, expressed from their endogenous promoters. We found that both the WT and suppressor versions interacted with Mcp1 (Fig. 3 A). Mcp1 is a membrane protein with five predicted transmembrane domains. Only short regions that stick out of the membrane could potentially interact with Vps13 (Fig. 3 C). To assess which part of Mcp1 interacted with Vps13, we first assessed Mcp1 topology by exposing purified mitochondria overexpressing C-terminally HA-tagged Mcp1 to increasing amounts of proteinase K (PK). We then detected protected fragments by Western blotting, using either an anti-HA antibody to detect the C terminus or an antibody raised against the N terminus of Mcp1 (aa 20–40). At small amounts of PK, both antibodies detected the appearance of fragments of 20 kD (Fig. 3 B), indicating cleavage at the level of loop 2 and an N-out, C-in conformation for Mcp1 (Fig. 3 C). Interestingly, the N-terminal fragment remained protease resistant even at large PK concentrations, suggesting either that the epitope was too close to the membrane to be accessible to PK or that this domain is tightly folded. An N-out, C-in conformation indicated that two domains could potentially interact with Vps13, namely, the

N terminus (aa 1–61) and loop 2 (aa 122–173), whereas loop 4 appeared too short to serve as a binding site. To assess if any of these fragments was binding to Vps13, we adopted a relocalization approach in which we targeted these two segments of Mcp1 to the ER (Fig. 3 D) and asked if Vps13 follows any of these segments. Strikingly, expressing the N terminus fused to an ER-targeted red fluorescent protein (mCherry–Ubc6) led to the recruitment of Vps13 to the ER. The same effect was not observed for the fusion protein containing loop 2 (Fig. 3 D). Thus, the N-terminal fragment (1–61 aa) of Mcp1 was sufficient for the binding of Vps13 and its recruitment to a foreign organelle.

Suppressor mutations identified in Vps13 all cluster to the repeat-containing domains (Lang et al., 2015; Park et al., 2016). We wondered if these domains or any other region was involved in Mcp1-mediated recruitment. To this aim, we performed a series of N- and C-terminal truncations on the endogenous Vps13 and asked if the truncated versions were still able to localize to mitochondria upon Mcp1 overexpression. Vps13 C-terminally truncated up to aa 2,599 was robustly recruited to mitochondria. Shorter truncations remained, however, mostly cytoplasmic (Fig. 3, E and F). Short N-terminal truncations destabilized the protein, such that their localization was difficult to assess. However, a larger deletion up to aa 2,247 was recruited to the mitochondria. Even though, in this case, the fluorescence levels were low, the mitochondrial localization was evident only in MCP1 overexpression conditions (Fig. 3 E, bottom). Thus, the Mcp1-binding region (aa 2,247–2,599) of Vps13 does not overlap with the region harboring suppressor mutations, in agreement with the fact that the suppressor mutation does not act by increasing Vps13/Mcp1 interaction (Fig. 3 A). Dominant suppressor mutations therefore probably act by relieving an inhibitory activity in Vps13 (Lang et al., 2015), without affecting its mitochondrial recruitment.

Having established the key elements of Mcp1-Vps13 interaction, we asked if the only function of Mcp1 in the ERM ES-bypass pathway is to recruit Vps13 to mitochondria. To test this, we constructed a minimal mitochondrial recruiting fragment by fusing aa 1–61 of Mcp1 to an outer mitochondrial membrane-targeted red fluorescent protein (mCherry–Fis1) and asked whether its expression could suppress the phenotype of the *mmm1-1* ts strain at the restrictive temperature. The expression of this construct, but not of mCherry–Fis1 alone, led to the strong recruitment of Vps13 to mitochondria (Fig. 4 A). However, the growth phenotype was not rescued at 37°C upon the loss of functional Mmm1 (Fig. 4 B). This was not due to a failure of Mcp1 (1–61 aa) to recruit Vps13 onto mitochondria in ERMES mutant conditions, as Vps13 was recruited to mitochondria even at the restrictive temperature (Fig. 4 A, right). In fact, *mmm1-1* ts strain expressing the Mcp1 (1–61 aa) construct grew worse than the nonexpressing parent, indicating that the nonfunctional fragment likely titrated Vps13 away from the functional, full-length Mcp1 (Fig. 4 B). We conclude that Vps13 recruitment to mitochondria is necessary but not sufficient to rescue the loss of ERMES function. Thus, full-length Mcp1, in addition to recruiting Vps13, plays an active role in the ERMES bypass pathway. Indeed, a hidden Markov model homology analysis (HHPred) suggested that Mcp1 might fold as a five-helix bundle, as in succinate dehydrogenase and quinol–fumarate reductases (Alignment S4), pointing to a role beyond the mere recruitment of Vps13. We used homology modeling to construct a model of MCP1. The homology started at aa 45 of Mcp1, that is, close to the first transmembrane region, and extended until the end of the protein. In the model, four histidines (H72, H114, H187, and H237) constituted two putative heme-binding domains (Fig. 4 C), as in the quinol fumarate reductase from *Wolinella succinogenes*, which served as a template for homology modeling. Mcp1 is conserved within a subgroup of ascomycetes. Therefore, to address if heme binding is a conserved feature of Mcp1, we aligned *MCP1* in several fungi. Although the homology was generally good within transmembrane domains, the presumptive heme-binding histidines were among the completely conserved amino acids, suggesting that heme binding is an important feature of Mcp1 (Fig. 4 D). Indeed, mutating histidine residues in either presumptive heme-binding domains (H187A and H237A, respectively) severely blunted the ability of Mcp1 to rescue ERMES defects when overexpressed (Fig. 4 E), without affecting Vps13 recruitment to mitochondria (Fig. 4 F). Mutating other conserved residues (P195A and G241A) yielded variable outcomes on ERMES rescue but did not affect Vps13 recruitment, as expected.

In summary, Vps13 and Mcp1 interact either directly or indirectly on the mitochondrial surface. This interaction is necessary for the ERMES bypass pathway, but merely bringing Vps13 to mitochondria is not sufficient, and presumptive heme-binding domains are important for the ERMES-rescue phenomenon.

How does this bypass work? It is logical that an MCS can be bypassed by another MCS, and in this case, vacuole–mitochondria contacts might serve as an alternative MCS. Indeed, both Vps13- and Mcp1-mediated suppression require Vps39 (Lang et al., 2015; Fig. 2 C). However, two observations challenge the idea that vacuole–mitochondria contacts are involved in ERMES suppression. First, vCLAMP formation through Vps39 overexpression does not alter Vps13 localization (Fig. 2 B). Conversely, neither the Vps13 suppressor alleles nor Mcp1 overexpression induces the formation of vCLAMPs (Lang et al., 2015; Fig. 2 D).

In an effort to resolve this paradox, we co-overexpressed Vps39 and Mcp1 in cells expressing Vps13^GFP. In this case, Vps13 was not only recruited to mitochondria by Mcp1 but was robustly enriched at Vps39 overexpression-mediated vCLAMPs (Fig. 5 A).

Discussion

Here we show that Mcp1 and Vps13 interact at vacuole–mitochondria interfaces and require Vps39 function in the ERMES-bypass pathway. What is the relationship among these three factors? Unlike the overexpression of Mcp1 or the expression of the Vps13 suppressor, the overexpression of Vps39, despite causing the formation of vCLAMPs, is incapable of reverting ERMES growth phenotype (Fig. 2, E and F), in contrast to previously reported findings (Hönscher et al., 2014). In contrast, Mcp1- and Vps13-mediated ERMES rescue happens in conditions in which vacuole–mitochondria contacts are not enlarged into vCLAMPs. These results indicate that the amount and activity of Vps13 targeted to mitochondria, but not the enhanced surface of contact between the organelles, are limiting for the output of the bypass pathway.

Vps13 is enriched at vCLAMPs only when both Vps39 and Mcp1 are co-overexpressed. This suggests that when Vps39 overexpression mediates vCLAMP formation, Vps13 fails to accumulate there, because Mcp1 is limiting for its recruitment to mitochondria. Conversely, when Mcp1 overexpression

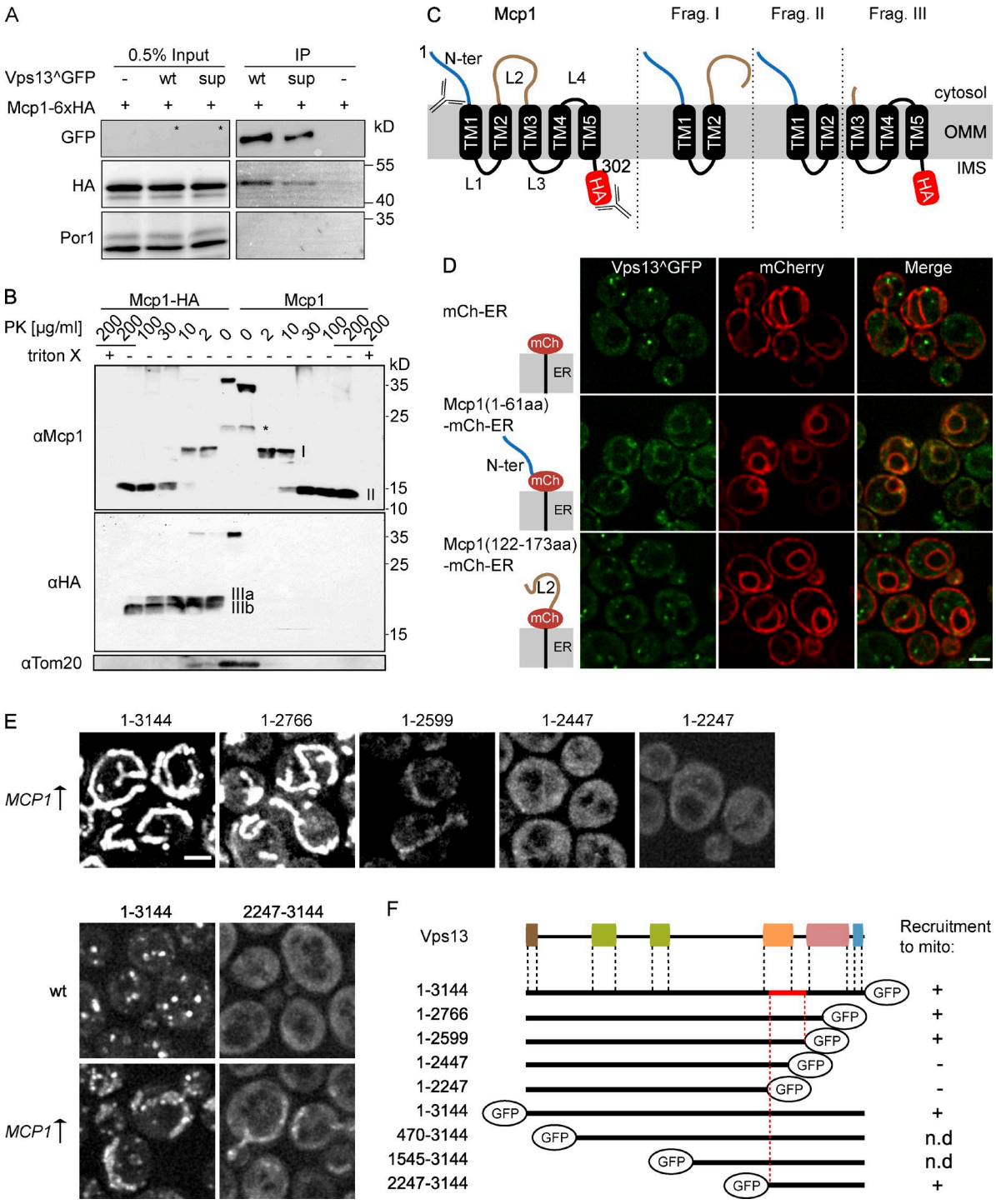

Figure 3. **Mcp1 recruits Vps13 to mitochondria.** (A) Cells expressing Vps13^GFP (WT or suppressor) along with HA-tagged Mcp1 were subjected to immunoprecipitation (IP) using GFP–TrapA beads. Eluates from the beads were analyzed by SDS-PAGE and Western blotting using antibodies against GFP, HA, or yeast porin, Por1 (negative control). Note that the GFP antibody did not detect endogenous Vps13 in whole-cell lysates (asterisks). (B) PK accessibility assay. Isolated mitochondria were incubated in presence of the indicated amounts of PK and then subjected to Western blotting with the indicated antibodies. Proteolytic fragments I, II, and III are indicated. Asterisk denotes uncharacterized PK-independent fragment. (C) Topology of Mcp1 and proteolytic fragments on the outer mitochondrial membrane (OMM). Mcp1 bears five transmembrane (TM) helices (TM1–TM5) and four loops (L1–L4). The cytosol-exposed N terminus (aa 1–61) and L2 (aa 122–173) are shown in blue and brown, respectively. IMS, intermembrane space. (D) Localization of endogenous Vps13 (green) with ER-targeted mCherry alone or fused to the indicated Mcp1 fragments, expressed from a plasmid. (E) Mapping the Mcp1-binding region of Vps13. (Top) Localization of full-length Vps13 and the indicated truncations C-terminally tagged with GFP, upon Mcp1 overexpression. (Bottom) Localization of full-length Vps13 and the indicated truncated version N-terminally tagged with GFP, under normal conditions and Mcp1 overexpression. The expression of the N-terminal truncations was driven by the CYC1 promoter. All truncations were performed genomically. (F) Schematic representation of C-terminal and N-terminal truncations and their mitochondrial recruitment upon Mcp1 overexpression. The region of interaction with Mcp1 lies between aa 2,247 and 2,599. n.d., not determined. Bars, 2 µm.

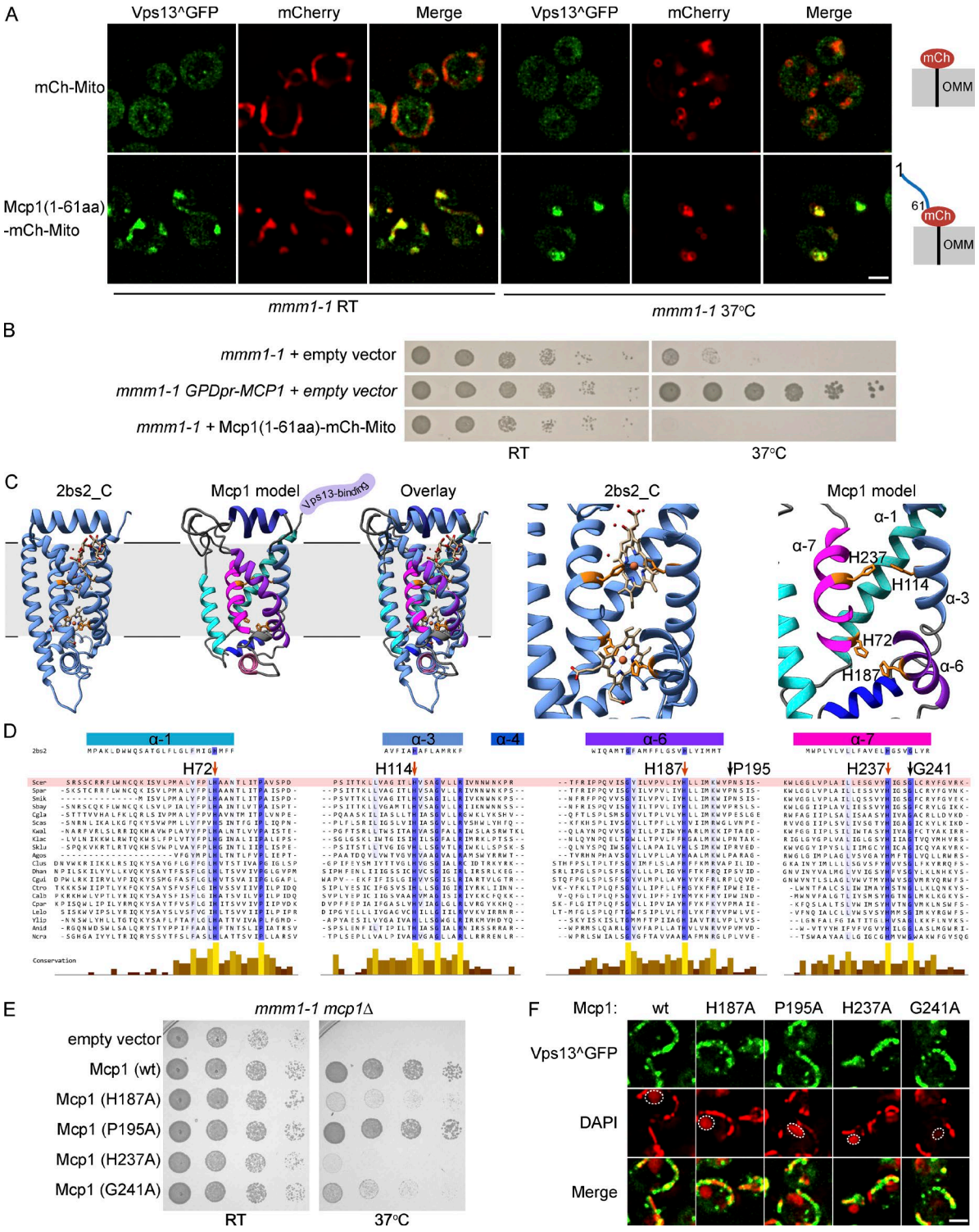

Figure 4. **Mcp1 has additional functions besides recruiting Vps13.** (A) Cells coexpressing Vps13^GFP and either mitochondria-targeted mCherry alone or mCherry fused to the Mcp1 fragment 1–61 were grown at RT (left). To inactivate Mmm1, cells were shifted to 37°C for 2 h and imaged (right). Note the altered mitochondrial morphology at the restrictive temperature. OMM, outer mitochondrial membrane. (B) The *mmm1-1* ts strains carrying an empty vector or the vector bearing the Mcp1 fragment 1–61 were spotted as serial dilutions on SD-HIS plates and grown for 2 d either at RT or 37°C. The *mmm1-1* ts strain with Mcp1 overexpression along with empty vector served as a positive control for growth rescue at the restrictive temperature. (C, top) The structure of the membrane-spanning component of the fumarate quinol reductase from *W. succinogenes* (left; Protein Data Bank 2BS2) was used for homology modeling of Mcp1. (Right) Magnification of the heme-binding sites in the fumarate quinol reductase and their predicted location in Mcp1. (D) Alignment of Mcp1 α-helices 1, 3, 6, and 7 in different ascomycetes orthologues. (E) *mmm1-1* ts *mcp1Δ* cells transformed with plasmids overexpressing WT or mutant Mcp1 were spotted as serial dilutions and grown at either RT or 37°C. (F) Live cells expressing Vps13^GFP and overexpressing indicated mutants of Mcp1 were counterstained with DAPI to reveal mitochondria and nuclei (dashed lines). Bars, 2 µm.

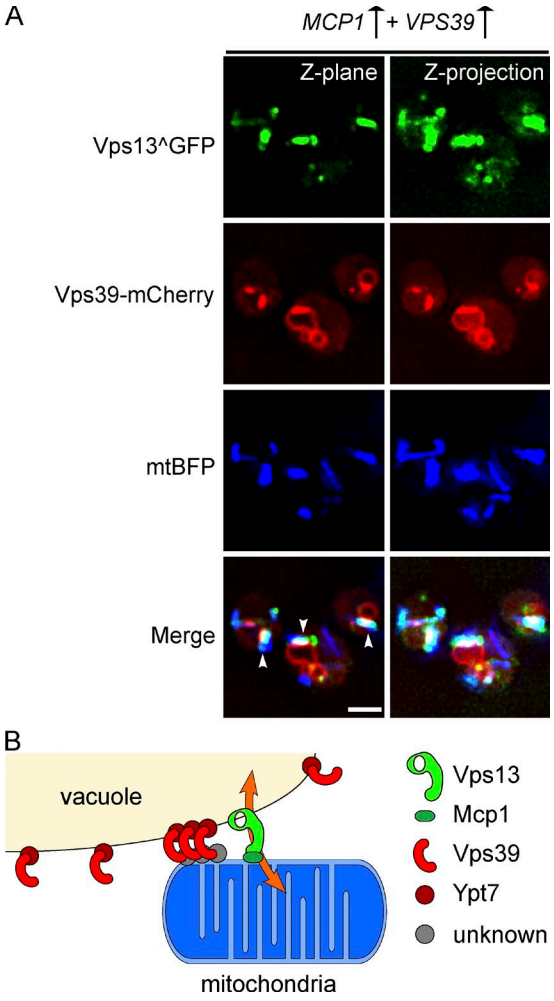

Figure 5. **Recruitment of Vps13 to vCLAMPs upon Vps39 and Mcp1 co-overexpression.** (A) Vps39 is genomically tagged with mCherry at its C terminus. Mitochondria are marked by a plasmid-encoded, matrix-targeted BFP (mtBFP). A single Z-section and a maximum intensity projection of five Z-sections are shown. White arrowheads point at vCLAMPs. Bar, 2 µm. (B) Proposed model for the mechanism of the ERMES-bypass pathway. The recruitment of the vCLAMP factor Vps39 by the Rab GTPase Ypt7 anchors the vacuole to mitochondria via a yet unknown mitochondrial factor. This anchoring facilitates the recruitment of Vps13 to vacuole–mitochondria contacts sites by the outer mitochondrial membrane protein Mcp1. These two proteins potentially act in tandem to function as effectors of vacuole–mitochondria contacts.

recruits Vps13 to mitochondria, Vps13 is not visibly enriched at vacuole–mitochondria contacts, because the surface of contact between both organelles is limiting.

A model that reconciles our observations is that Vps39 acts as a vacuole–mitochondria tether, while Vps13 and Mcp1 act as physiological effectors of vacuole–mitochondria MCSs function, which can compensate for the absence of ERMES (Fig. 5 B). In this case, the tethering and physiological output of vacuole–mitochondria MCSs would be performed by separate factors. Such a division of labor between tethers and effectors at MCSs is novel, as most MCS proteins described so far harbor both tethering and physiological effector activities. For instance, ERMES has an important tethering activity but also harbors lipid exchange proteins (Kornmann et al., 2009; Ah-Young et al., 2015; Jeong et al., 2016). The same is true for extended synaptotagmins, which both tether the ER to the plasma membrane and transport lipids (Manford et al., 2012; Schauder et al., 2014; Saheki et al., 2016).

Consistent with biochemical tethering activity, Vps39 is a known member of the homotypic fusion and protein sorting complex, which is involved in the tethering of late endosomes and vacuoles (Bröcker et al., 2012). By contrast, Vps13 is known to function at MCSs that are tethered by other factors, for instance, nuclear–vacuole junctions tethered by Nvj1 and Vac8 (Pan et al., 2000).

Our elucidation of the mechanism of suppression by the Mcp1-Vps13-Vps39 module supports previous findings (Elbaz-Alon et al., 2014; Hönscher et al., 2014) and firmly establishes vacuole as a critical organelle involved in restoring mitochondrial homeostasis upon the loss of ER–mitochondria contacts. Although endosome–mitochondria (Park et al., 2016) and peroxisome–mitochondria contacts might play a role in ERMES compensation, our data suggest that neither a fully functional endocytic pathway nor functional peroxisomes are required for this purpose (Fig. 2 C).

Because a core function of ERMES appears to be lipid exchange and because Mcp1 and Vps13 serve as effectors of vacuole–mitochondria contacts, it is tempting to speculate that these two proteins are directly involved in lipid transport. Unlike well-characterized lipid transport proteins that localize to organelle contact sites, Vps13 does not seem to harbor any known lipid transport domains based on sequence alignments. However, because only low-resolution structures of Vps13 are available (De et al., 2017), it cannot be excluded that Vps13 harbors a yet uncharacterized lipid transport domain. In the case of Mcp1, our data point to an important role for the membrane-embedded part of Mcp1. This segment likely folds as a heme-binding five-helix bundle, as in quinol–fumarate reductases. This domain might be involved in lipid extraction from and/or lipid insertion into the outer mitochondrial membrane. Whether heme binding serves oxidoreductive roles is unknown. Because Mcp1 is present only in a subset of ascomycetes, and because the five-helix bundle of Mcp1 resembles that found in the succinate dehydrogenases of gram-positive bacteria, it appears that Mcp1 is the result of a recent horizontal gene transfer. It is thus possible that heme binding serves only a structural role in Mcp1. Consistent with this idea, overexpressing a mutant protein presumably incapable of binding heme did severely blunt, but did not entirely abrogate, the activity of Mcp1 in the ERMES-bypass pathway (Fig. 4 E). Of note, succinate dehydrogenases and fumarate reductases use quinols and quinones as electron donors and acceptors and bind these lipids in dedicated cavities at the interface with the lipid bilayer. This lipid-binding ability might be exploited in the ERMES bypass pathway to favor the desorption of phospholipids from the membrane. Alternatively, it is conceivable that Mcp1 and Vps13 cooperate to recruit lipid transport proteins that are yet to be identified.

Could the ERMES bypass pathway be conserved in metazoans? Like ERMES subunits, Mcp1 is not conserved. However, Vps13 is highly conserved with four paralogs, Vps13A-D, in humans. Mutations in these genes are associated with different neurological disorders (Ueno et al., 2001; Kolehmainen et al., 2003; Tomiyasu et al., 2011). In particular, mutation in VPS13C, associated with a form of Parkinson's disease, is linked to mitochondrial dysfunction (Lesage et al., 2016). Given that a short amino acid stretch alone is sufficient to recruit Vps13 to mitochondria, it is conceivable that Mcp1 function has been

substituted by another mitochondrial protein in metazoans, despite low sequence conservation. Therefore, by shedding light on the mechanism of Vps13 recruitment and its function in vacuole/lysosome–mitochondria contact sites, our study has taken an important step toward understanding the function of the mitochondrial pool of Vps13 in health and disease.

Materials and methods

Yeast strains and plasmids

Strains used in this study are listed in Table S1. Genomic integration of PCR fragments was performed by homologous recombination (Puig et al., 1998; Janke et al., 2004; Gauss et al., 2005). Gene deletions were confirmed by colony PCR. Plasmids and primers used in the study are listed in Tables S2 and S3, respectively. mCherry was targeted to the ER by C-terminal fusion of aa 230–250 of Ubc6. Targeting to mitochondria was achieved by C-terminal fusion of aa 132–155 of Fis1. Plasmids bearing MCP1 fragments with mCherry targeted to the ER or mitochondria were constructed using the Gibson Assembly cloning kit (New England Biolabs). To generate the plasmid bearing GFP-tagged Vps13 after aa 499, the pSOI1 plasmid (Brickner and Fuller, 1997) bearing the full-length VPS13 sequence was digested and gap-repaired in a yeast strain bearing the GFP-tagged *VPS13* in the genome (Lang et al., 2015).

Growth assay

Cells were grown in yeast extract peptone dextrose or minimal medium to mid-log phase, diluted to 0.25 OD_{600}, spotted on appropriate plates, and grown at RT or 37°C. Fivefold serial dilutions were made, with the first spot in each row corresponding to 2.5 µl of 0.25 OD_{600}.

PK accessibility assay

Mitochondria were isolated from yeast cells expressing either Mcp1-HA or Mcp1 by differential centrifugation as described before (Daum et al., 1982). Mitochondria (50 µg) were treated with increasing amounts (2–200 µg/ml) of PK in the absence or presence of 1% Triton X-100. Samples were analyzed using SDS-PAGE followed by Western blot analysis with antibodies against Mcp1, the HA tag, or the indicated mitochondrial proteins.

GFP immunoprecipitation

Approximately 1,500 OD units of cells grown overnight in yeast extract peptone dextrose were resuspended in 2 ml TNG buffer (50 mM Tris, pH 7.4, 100 mM NaCl, and 5% glycerol) together with protease inhibitors pepstatin and aprotinin at a final concentration of 1 µg/ml. Glass beads were added, and cells were lysed using a Disrupter Genie (Scientific Industries) for 10 min at 4°C. The lysate was centrifuged at 13,000 *g* for 5 min, and the supernatant was collected. To the pellet, 700 µl of TNG buffer with 1% NP-40 was added, resuspended, and left on a nutator at 4°C for 30 min. After centrifugation, the supernatants were pooled, and the protein amount was estimated. 20 µl GFP–TrapA beads (ChromoTek) were added and left on a nutator at 4°C for 4 h. After washing the beads (50 mM Tris, pH 7.4, 400 mM NaCl, and 5% glycerol), bound proteins were eluted with 1× Laemmli buffer with incubation at 42°C for 15 min.

Fluorescence microscopy

Cells were grown to mid-log phase in complete synthetic dextrose (SD) medium or SD–uracil (for selection for mitochondrial blue fluorescent protein plasmid) or SD–uracil–leucine (for selection of mitochondrial blue fluorescent protein and the Vps13^GFP plasmids). Images were acquired using a DeltaVision MPX microscope (Applied Precision) equipped with a 100× 1.40 NA oil UplanS-Apo objective lens (Olympus), a multicolor illumination light source, and a CoolSNAPHQ2 camera (Roper Scientific). Image acquisition was done at RT. Images were deconvolved with SoftWoRx software using the manufacturer's parameters. Images were processed further using FIJI ImageJ bundle and assembled on Adobe Illustrator CS6. A single Z-section is depicted in the figures unless otherwise mentioned. For vacuolar staining, cells were pulsed with FM4-64 (Molecular Probes) at a concentration of 5 µg/ml for 20 min in the dark at 30°C. After washing, cells were chased for another 20 min in medium without FM4-64 and imaged subsequently. Quantification of colocalization was performed automatically in ImageJ (see the scripts in the online supplemental material).

Bioinformatics analyses

Hidden Markov model homology searches were performed using HHpred software (Söding et al., 2005). Homology modeling was performed using the Swiss-Model server (Biasini et al., 2014). 3D protein structures were rendered using tCHIMERA software (Pettersen et al., 2004).

Online supplemental material

Fig. S1 shows that Pex10 and Vps38 do not colocalize. Fig. S2 shows that the Vps13 suppressor rescues loss of ERMES function in the absence of Vps38. Yeast strains, plasmids, and primers used in the study are listed in Tables S1, S2, and S3, respectively. Alignments S1 and S2 show homology search results for Vps13 (1–3,000 aa) and Vps13 (1,501–3,144 aa), searched against the Pfam database and yeast proteome, respectively. Alignments S3 and S4 show the results for the C terminus of Vps13 (3,030–3,144 aa) and full-length Mcp1, respectively, searched against the Protein Data Bank. All homology alignments were generated using the HHPred server. Scripts S1, S2, and S3 are ImageJ macros used to calculate the percentage of colocalization between Vps13^GFP/Pex10-mCherry foci, Vps13^GFP/Vps38-mCherry foci, and Pex10-GFP/Vps38-mCherry foci, respectively.

Acknowledgments

We are thankful to the Kornmann laboratory members for discussions and helpful suggestions. Imaging was done at the ETH Zürich ScopeM facility.

This work was supported by Schweizerischer Nationalfonds zur Förderung der Wissenschaftlichen Forschung (grant PP00P3_133651) and the H2020 European Research Council (ERC-2013-StG 337906-OrgaNet) to B. Kornmann. D. Antunes was supported by the International Max Planck Research Schools "From Molecules to Organisms" (Tuebingen, Germany).

The authors declare no competing financial interests.

Author contributions: A.T. John Peter and B. Kornmann conceived and designed the experiments. A.T. John Peter performed the experiments, except the experiments in Fig. 3, D and E (designed and performed by B. Hermann and A.T. John Peter); Fig. 3 B (designed by D. Antunes, D. Rapaport, and K.S. Dimmer and performed by D. Antunes); and Fig. 4, E and F (designed by D. Antunes, D. Rapaport, and K.S. Dimmer and performed by D. Antunes and A.T. John Peter). A.T. John Peter and B. Kornmann wrote the paper with input from D. Antunes and D. Rapaport.

Submitted: 17 October 2016
Revised: 26 June 2017
Accepted: 25 July 2017

References

AhYoung, A.P., J. Jiang, J. Zhang, X. Khoi Dang, J.A. Loo, Z.H. Zhou, and P.F. Egea. 2015. Conserved SMP domains of the ERMES complex bind phospholipids and mediate tether assembly. *Proc. Natl. Acad. Sci. USA*. 112:E3179–E3188. http://dx.doi.org/10.1073/pnas.1422363112

Biasini, M., S. Bienert, A. Waterhouse, K. Arnold, G. Studer, T. Schmidt, F. Kiefer, T. Gallo Cassarino, M. Bertoni, L. Bordoli, and T. Schwede. 2014. SWISS-MODEL: Modelling protein tertiary and quaternary structure using evolutionary information. *Nucleic Acids Res.* 42:W252–W258. http://dx.doi.org/10.1093/nar/gku340

Brickner, J.H., and R.S. Fuller. 1997. SOI1 encodes a novel, conserved protein that promotes TGN-endosomal cycling of Kex2p and other membrane proteins by modulating the function of two TGN localization signals. *J. Cell Biol.* 139:23–36. http://dx.doi.org/10.1083/jcb.139.1.23

Bröcker, C., A. Kuhlee, C. Gatsogiannis, H.J. Balderhaar, C. Hönscher, S. Engelbrecht-Vandré, C. Ungermann, and S. Raunser. 2012. Molecular architecture of the multisubunit homotypic fusion and vacuole protein sorting (HOPS) tethering complex. *Proc. Natl. Acad. Sci. USA*. 109:1991–1996. http://dx.doi.org/10.1073/pnas.1117797109

Collins, S.R., A. Roguev, and N.J. Krogan. 2010. Quantitative genetic interaction mapping using the E-MAP approach. *Methods Enzymol.* 470:205–231. http://dx.doi.org/10.1016/S0076-6879(10)70009-4

Costanzo, M., A. Baryshnikova, J. Bellay, Y. Kim, E.D. Spear, C.S. Sevier, H. Ding, J.L.Y. Koh, K. Toufighi, S. Mostafavi, et al. 2010. The genetic landscape of a cell. *Science.* 327:425–431. http://dx.doi.org/10.1126/science.1180823

Daum, G., P.C. Böhni, and G. Schatz. 1982. Import of proteins into mitochondria. Cytochrome b2 and cytochrome c peroxidase are located in the intermembrane space of yeast mitochondria. *J. Biol. Chem.* 257:13028–13033.

De, M., A.N. Oleskie, M. Ayyash, S. Dutta, L. Mancour, M.E. Abazeed, E.J. Brace, G. Skiniotis, and R.S. Fuller. 2017. The Vps13p-Cdc31p complex is directly required for TGN late endosome transport and TGN homotypic fusion. *J. Cell Biol.* 216:425–439. http://dx.doi.org/10.1083/jcb.201606078

Elbaz-Alon, Y., E. Rosenfeld-Gur, V. Shinder, A.H. Futerman, T. Geiger, and M. Schuldiner. 2014. A dynamic interface between vacuoles and mitochondria in yeast. *Dev. Cell.* 30:95–102. http://dx.doi.org/10.1016/j.devcel.2014.06.007

Ellenrieder, L., Ł. Opaliński, L. Becker, V. Krüger, O. Mirus, S.P. Straub, K. Ebell, N. Flinner, S.B. Stiller, B. Guiard, et al. 2016. Separating mitochondrial protein assembly and endoplasmic reticulum tethering by selective coupling of Mdm10. *Nat. Commun.* 7:13021. http://dx.doi.org/10.1038/ncomms13021

Fidler, D.R., S.E. Murphy, K. Courtis, P. Antonoudiou, R. El-Tohamy, J. Ient, and T.P. Levine. 2016. Using HHsearch to tackle proteins of unknown function: A pilot study with PH domains. *Traffic.* 17:1214–1226. http://dx.doi.org/10.1111/tra.12432

Gauss, R., M. Trautwein, T. Sommer, and A. Spang. 2005. New modules for the repeated internal and N-terminal epitope tagging of genes in Saccharomyces cerevisiae. *Yeast*. 22:1–12. http://dx.doi.org/10.1002/yea.1187

Helle, S.C.J., G. Kanfer, K. Kolar, A. Lang, A.H. Michel, and B. Kornmann. 2013. Organization and function of membrane contact sites. *Biochim. Biophys. Acta.* 1833:2526–2541. http://dx.doi.org/10.1016/j.bbamcr.2013.01.028

Hönscher, C., M. Mari, K. Auffarth, M. Bohnert, J. Griffith, W. Geerts, M. van der Laan, M. Cabrera, F. Reggiori, and C. Ungermann. 2014. Cellular metabolism regulates contact sites between vacuoles and mitochondria. *Dev. Cell.* 30:86–94. http://dx.doi.org/10.1016/j.devcel.2014.06.006

Hoppins, S., S.R. Collins, A. Cassidy-Stone, E. Hummel, R.M. Devay, L.L. Lackner, B. Westermann, M. Schuldiner, J.S. Weissman, and J. Nunnari. 2011. A mitochondrial-focused genetic interaction map reveals a scaffold-like complex required for inner membrane organization in mitochondria. *J. Cell Biol.* 195:323–340. http://dx.doi.org/10.1083/jcb.201107053

Huh, W.-K., J.V. Falvo, L.C. Gerke, A.S. Carroll, R.W. Howson, J.S. Weissman, and E.K. O'Shea. 2003. Global analysis of protein localization in budding yeast. *Nature.* 425:686–691. http://dx.doi.org/10.1038/nature02026

Janke, C., M.M. Magiera, N. Rathfelder, C. Taxis, S. Reber, H. Maekawa, A. Moreno-Borchart, G. Doenges, E. Schwob, E. Schiebel, and M. Knop. 2004. A versatile toolbox for PCR-based tagging of yeast genes: New fluorescent proteins, more markers and promoter substitution cassettes. *Yeast*. 21:947–962. http://dx.doi.org/10.1002/yea.1142

Jeong, H., J. Park, and C. Lee. 2016. Crystal structure of Mdm12 reveals the architecture and dynamic organization of the ERMES complex. *EMBO Rep.* 17:1857–1871. http://dx.doi.org/10.15252/embr.201642706

Kihara, A., T. Noda, N. Ishihara, and Y. Ohsumi. 2001. Two distinct Vps34 phosphatidylinositol 3-kinase complexes function in autophagy and carboxypeptidase Y sorting in *Saccharomyces cerevisiae*. *J. Cell Biol.* 152:519–530. http://dx.doi.org/10.1083/jcb.152.3.519

Knoops, K., R. de Boer, A. Kram, and I.J. van der Klei. 2015. Yeast pex1 cells contain peroxisomal ghosts that import matrix proteins upon reintroduction of Pex1. *J. Cell Biol.* 211:955–962. http://dx.doi.org/10.1083/jcb.201506059

Kolehmainen, J., G.C.M. Black, A. Saarinen, K. Chandler, J. Clayton-Smith, A.-L. Träskelin, R. Perveen, S. Kivitie-Kallio, R. Norio, M. Warburg, et al. 2003. Cohen syndrome is caused by mutations in a novel gene, COH1, encoding a transmembrane protein with a presumed role in vesicle-mediated sorting and intracellular protein transport. *Am. J. Hum. Genet.* 72:1359–1369. http://dx.doi.org/10.1086/375454

Kopec, K.O., V. Alva, and A.N. Lupas. 2010. Homology of SMP domains to the TULIP superfamily of lipid-binding proteins provides a structural basis for lipid exchange between ER and mitochondria. *Bioinformatics.* 26:1927–1931. http://dx.doi.org/10.1093/bioinformatics/btq326

Kornmann, B., E. Currie, S.R. Collins, M. Schuldiner, J. Nunnari, J.S. Weissman, and P. Walter. 2009. An ER-mitochondria tethering complex revealed by a synthetic biology screen. *Science.* 325:477–481. http://dx.doi.org/10.1126/science.1175088

Lang, A.B., A.T. John Peter, P. Walter, and B. Kornmann. 2015. ER-mitochondrial junctions can be bypassed by dominant mutations in the endosomal protein Vps13. *J. Cell Biol.* 210:883–890. http://dx.doi.org/10.1083/jcb.201502105

Lesage, S., V. Drouet, E. Majounie, V. Deramecourt, M. Jacoupy, A. Nicolas, F. Cormier-Dequaire, S.M. Hassoun, C. Pujol, S. Ciura, et al. International Parkinson's Disease Genomics Consortium (IPDGC). 2016. Loss of VPS13C function in autosomal-recessive parkinsonism causes mitochondrial dysfunction and increases PINK1/Parkin-dependent mitophagy. *Am. J. Hum. Genet.* 98:500–513. http://dx.doi.org/10.1016/j.ajhg.2016.01.014

Luo, W., and A. Chang. 1997. Novel genes involved in endosomal traffic in yeast revealed by suppression of a targeting-defective plasma membrane ATPase mutant. *J. Cell Biol.* 138:731–746. http://dx.doi.org/10.1083/jcb.138.4.731

Manford, A.G., C.J. Stefan, H.L. Yuan, J.A. Macgurn, and S.D. Emr. 2012. ER-to-plasma membrane tethering proteins regulate cell signaling and ER morphology. *Dev. Cell.* 23:1129–1140. http://dx.doi.org/10.1016/j.devcel.2012.11.004

Mattoon, J.R., E. Caravajal, and D. Guthrie. 1990. Effects of hap mutations on heme and cytochrome formation in yeast. *Curr. Genet.* 17:179–183. http://dx.doi.org/10.1007/BF00312865

Obara, K., T. Sekito, and Y. Ohsumi. 2006. Assortment of phosphatidylinositol 3-kinase complexes—Atg14p directs association of complex I to the pre-autophagosomal structure in *Saccharomyces cerevisiae*. *Mol. Biol. Cell.* 17:1527–1539. http://dx.doi.org/10.1091/mbc.E05-09-0841

Pan, X., P. Roberts, Y. Chen, E. Kvam, N. Shulga, K. Huang, S. Lemmon, and D.S. Goldfarb. 2000. Nucleus-vacuole junctions in *Saccharomyces cerevisiae* are formed through the direct interaction of Vac8p with Nvj1p. *Mol. Biol. Cell.* 11:2445–2457. http://dx.doi.org/10.1091/mbc.11.7.2445

Park, J.-S., M.K. Thorsness, R. Policastro, L.L. McGoldrick, N.M. Hollingsworth, P.E. Thorsness, and A.M. Neiman. 2016. Yeast Vps13 promotes mitochondrial function and is localized at membrane contact sites. *Mol. Biol. Cell.* 27:2435–2449. http://dx.doi.org/10.1091/mbc.E16-02-0112

Pettersen, E.F., T.D. Goddard, C.C. Huang, G.S. Couch, D.M. Greenblatt, E.C. Meng, and T.E. Ferrin. 2004. UCSF Chimera—a visualization system for exploratory research and analysis. *J. Comput. Chem.* 25:1605–1612. http://dx.doi.org/10.1002/jcc.20084

Phillips, M.J., and G.K. Voeltz. 2016. Structure and function of ER membrane contact sites with other organelles. *Nat. Rev. Mol. Cell Biol.* 17:69–82. http://dx.doi.org/10.1038/nrm.2015.8

Puig, O., B. Rutz, B.G. Luukkonen, S. Kandels-Lewis, E. Bragado-Nilsson, and B. Séraphin. 1998. New constructs and strategies for efficient PCR-based gene manipulations in yeast. *Yeast*. 14:1139–1146. http://dx.doi.org/10.1002/(SICI)1097-0061(19980915)14:12<1139::AID-YEA306>3.0.CO;2-B

Saheki, Y., X. Bian, C.M. Schauder, Y. Sawaki, M.A. Surma, C. Klose, F. Pincet, K.M. Reinisch, and P. De Camilli. 2016. Control of plasma membrane lipid homeostasis by the extended synaptotagmins. *Nat. Cell Biol.* 18:504–515. http://dx.doi.org/10.1038/ncb3339

Schauder, C.M., X. Wu, Y. Saheki, P. Narayanaswamy, F. Torta, M.R. Wenk, P. De Camilli, and K.M. Reinisch. 2014. Structure of a lipid-bound extended synaptotagmin indicates a role in lipid transfer. *Nature.* 510:552–555. http://dx.doi.org/10.1038/nature13269

Söding, J., A. Biegert, and A.N. Lupas. 2005. The HHpred interactive server for protein homology detection and structure prediction. *Nucleic Acids Res.* 33(Web Server):W244–W248. http://dx.doi.org/10.1093/nar/gki408

Tan, T., C. Ozbalci, B. Brügger, D. Rapaport, and K.S. Dimmer. 2013. Mcp1 and Mcp2, two novel proteins involved in mitochondrial lipid homeostasis. *J. Cell Sci.* 126:3563–3574. http://dx.doi.org/10.1242/jcs.121244

Tomiyasu, A., M. Nakamura, M. Ichiba, S. Ueno, S. Saiki, M. Morimoto, J. Kobal, Y. Kageyama, T. Inui, K. Wakabayashi, et al. 2011. Novel pathogenic mutations and copy number variations in the VPS13A gene in patients with chorea-acanthocytosis. *Am. J. Med. Genet. B. Neuropsychiatr. Genet.* 156B:620–631. http://dx.doi.org/10.1002/ajmg.b.31206

Ueno, S., Y. Maruki, M. Nakamura, Y. Tomemori, K. Kamae, H. Tanabe, Y. Yamashita, S. Matsuda, S. Kaneko, and A. Sano. 2001. The gene encoding a newly discovered protein, chorein, is mutated in chorea-acanthocytosis. *Nat. Genet.* 28:121–122. http://dx.doi.org/10.1038/88825

Velayos-Baeza, A., A. Vettori, R.R. Copley, C. Dobson-Stone, and A.P. Monaco. 2004. Analysis of the human VPS13 gene family. *Genomics*. 84:536–549. http://dx.doi.org/10.1016/j.ygeno.2004.04.012